Cement and Concrete Research 42 (2012) 710–720

Contents lists available at SciVerse ScienceDirect

Cement and Concrete Research

journal homepage: http://ees.elsevier.com/CEMCON/default.asp

Effect of grain size on the mechanical properties and crack formation of HPFRCC containing deformed steel fibers

Seok Hee Kang [a], Tae-Ho Ahn [b], Dong Joo Kim [a,*]

[a] Department of Civil and Environmental Engineering, Sejong University, 98 Gunja-Dong, Gwangjin-Gu, Seoul 143-747, Republic of Korea
[b] Innovative Construction Materials Engineering, Institute of Industrial Science, The University of Tokyo, 4-6-1 Komaba, Meguro-ku, Tokyo 153-8505, Japan

ARTICLE INFO

Article history:
Received 21 November 2011
Accepted 16 February 2012

Keywords:
Sand grain size (A)
Packing density (B)
Interfacial bond strength (C)
Strain hardening (C)
Cracking behavior (C)

ABSTRACT

This research investigated the influence of sand grain size on the behavior of high-performance fiber-reinforced cementitious composites (HPFRCC). Four types of sand with different grain sizes were investigated using the same matrix composition containing 2.0% hooked and twisted fibers by volume. The compressive strength was significantly greater for the finer sand grains, despite little difference in the packing density. The better compressive strength was mainly due to the denser calcium silicate hydrate (CSH) resulting from an intensive pozzolanic reaction with the finer silica sand, rather than to an improvement in packing density. The interfacial bond strength of those fibers was notably improved, having favorable effects on the mechanical properties and multiple crack formation of HPFRCCs. Although both fibers showed superior properties in mortars with a finer sand grain, twisted fiber produced more sensitive behavior according to the sand grain size.

1. Introduction

High performance fiber-reinforced cementitious composites (HPFRCC) are characterized by their unique tensile strain-hardening behavior accompanied by multiple micro cracks, as illustrated in Fig. 1 [3,7,21]. With their unique strain-hardening behavior, the use of HPFRCC provides a means of improving the load-carrying capacity and durability of civil infrastructure. However, because of their high cost, the use of HPFRCC is still not as widespread as would be expected based on their superior performance. Since even a 1% by volume fiber content is more expensive than matrix, minimizing the fiber content is an effective way of reducing the cost of HPFRCC. Silica sand (SS), which is normally used in HPFRCCs in preference to normal crushed sand (NS), is also more expensive than NS. Thus, from the cost point of view, the use of NS instead of SS in HPFRCC would represent a saving, provided that the tensile strain hardening behavior could be preserved.

To achieve tensile strain-hardening behavior using small amounts of fiber, the bond strength at the interface between fiber and matrix is extremely important. The interfacial bond strength is greatly influenced by the properties of the interfacial transition zone (ITZ) between fiber and matrix; thus, the properties of the ITZ in fiber-reinforced cement composites (FRCC) have a considerable effect on the mechanical properties of FRCC [1]. The interfacial bond strength is greatly influenced by the water–cement ratio as well as the sand content, while it is less sensitive to processing [19]. Guerrero and Naaman [18] reported that finer mortars, including fly ash and silica fume, had a significantly superior pullout resistance of steel fibers. The size of aggregate also has a significant effect on the microstructure of the ITZ in concrete, when viewed using scanning electron microscopy with backscattered electron imaging [2]. The influence of aggregate type and size on the mechanical behavior of engineered cementitious composite (ECC), one type of HPFRCC, was investigated by Sahmaran et al. [17]. The ECC mixtures with normal crushed limestone sand and gravel sand had a performance comparable to that of ECC that used micro silica sand. The type and size of sand grain are among the main parameters that influence the interfacial properties of the ITZ, especially in FRCC, hence they also have a significant effect on the interfacial bond strength. Thus, the overall tensile behavior of FRCC (or HPFRCC) with high-strength deformed steel fibers might also be expected to be influenced by the type and size of sand grain [6,11,14].

However, there are still insufficient data regarding the influence of sand grain size on the packing density of the mortar matrix, the effect of packing density on the interfacial bond strength, and the resulting overall tensile and flexural behavior of HPFRCC with high-strength deformed steel fibers. The aim of this research was to investigate the effect of sand grain size on the mechanical properties and crack formation of such HPFRCC. Specific objectives were: 1) to investigate the relationship between packing density and the compressive strength of mortar matrices in HPFRCC; 2) to investigate their interfacial bond properties and cracking behaviors under pullout, tensile and flexural tests; and 3) to discover any correlation between the fiber pullout mechanism and the sensitivity according to the size of sand grain.

* Corresponding author. Tel.: +82 2 3408 3820; fax: +82 2 3408 4332.
E-mail addresses: shkang1985@gmail.com (S.H. Kang), than@iis-u-tokyo.ac.jp (T.-H. Ahn), djkim75@sejong.ac.kr (D.J. Kim).

0008-8846/$ – see front matter © 2012 Elsevier Ltd. All rights reserved.
doi:10.1016/j.cemconres.2012.02.011

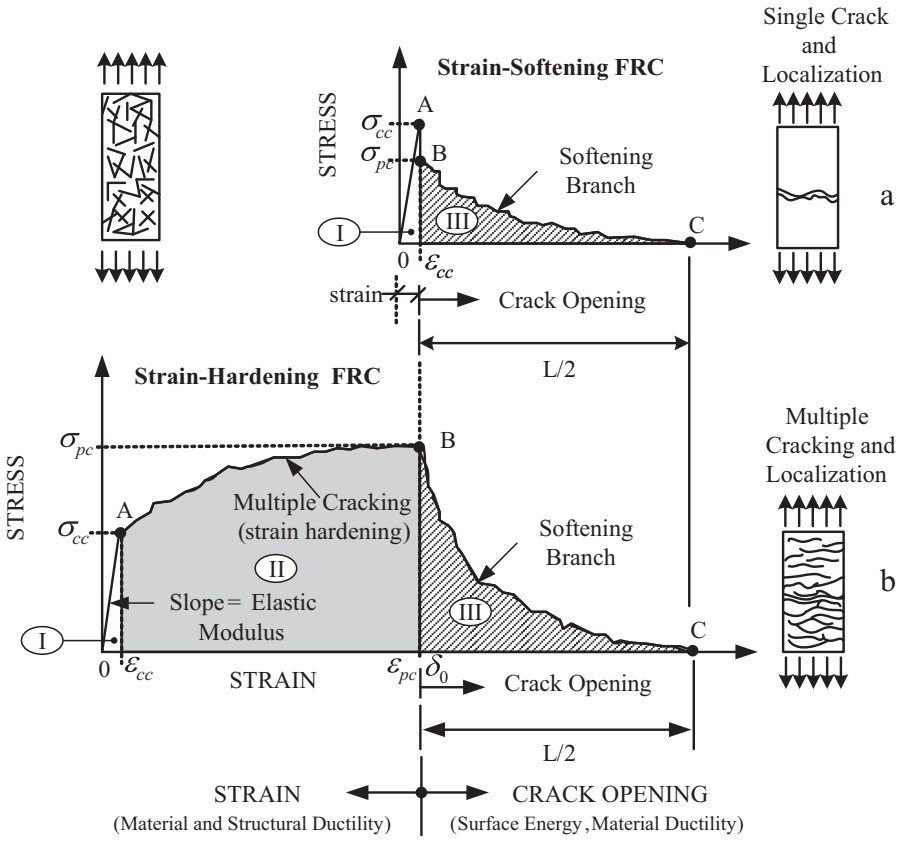

Fig. 1. Typical tensile strain softening and hardening behavior of FRC and HPFRCC [3,7].

Table 1
Composition of matrix mixtures by weight ratio and compressive strength.

Notation	Cement (type III)	Fly ash	Sand				Silica fume	Super-plasticizer	Water	Packing density	f_{ck} (MPa)
			NS	SS40	SS60	SS80					
Matrix A	0.80	0.20	1.00	–	–	–	0.07	0.018	0.26	0.733	76
Matrix B	0.80	0.20	–	1.00	–	–	0.07	0.015	0.26	0.737	89
Matrix C	0.80	0.20	–	–	1.00	–	0.07	0.019	0.26	0.739	103
Matrix D	0.80	0.20	–	–	–	1.00	0.07	0.040	0.26	0.745	120

2. Experimental program

An experimental program was designed to investigate the effect of sand grain size on the behavior of HPFRCC. First, the influence of sand grain size on the packing density and consequent compressive strength of the mortar matrix was investigated. The wet packing method proposed by Wong and Kwan [15] was used in estimating the packing density of mortar. Second, the influence of sand grain size on the interfacial bond strength of high-strength deformed steel fibers was investigated using single fiber pullout tests. Backscattered electron images were also obtained in order to visualize the interface between fiber and matrix according to the size of sand grain. Finally, both tensile and flexural test series were carried out to examine the mechanical and cracking behavior of HPFRCC according to different sand grain sizes in a matrix.

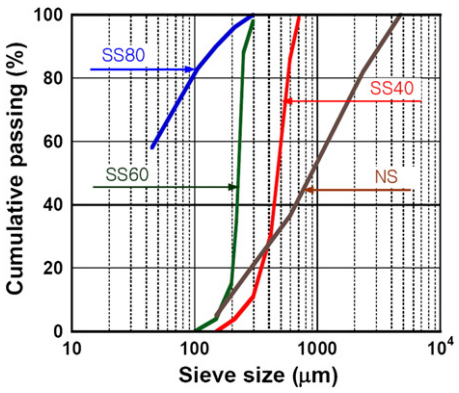

Fig. 2. Type of sand and cumulative passing ratio.

2.1. Materials and specimen preparation

Although all the matrices in this program had the same matrix compositions by weight ratio, as given in Table 1, they contained different

Table 2
Properties of fibers.

Name (notation)	Diameter (mm)	Length (mm)	Density (g/cm^3)	Tensile strength (MPa)	Elastic modulus (GPa)
Hooked (H-)	0.375	30	7.9	2311	200
Twisted (T-)	0.3[a]	30	7.9	2428[b]	200

[a] Equivalent diameter.
[b] Tensile strength of the fiber after twisting.

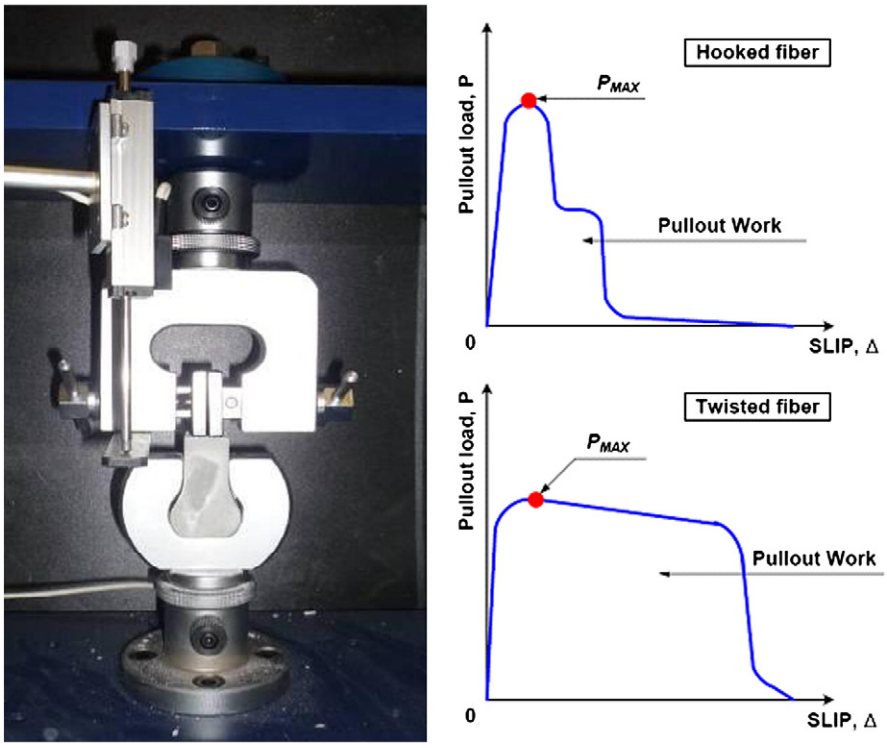

Fig. 3. Pullout test setup and parameters.

sizes of sand, as illustrated in Fig. 2. Matrix A contained normal crushed sand with a diameter range from 0.1 to 2.4 mm and an average of 0.7 mm (NS); Matrix B contained normal silica sand with a diameter range from 0.15 to 0.7 mm and an average of 0.42 mm (SS40); Matrix C contained fine micro silica sand with a diameter range from 0.1 to 0.3 mm and an average of 0.22 mm (SS60); and, Matrix D contained very fine micro silica sand with a diameter less than 0.2 mm (SS80). The compressive strength of mortar matrices according to the different types of sand is summarized in Table 1. High strength steel hooked (H-) and twisted (T-) fibers were investigated, and the volume content of fibers for both tension and flexural test specimens was 2.0%. The properties of those fibers are given in Table 2. The twisted fiber investigated had a triangular section, with three ribs per fiber length to avoid any fiber breakage during fiber pullout.

A mortar mixer was used to prepare the cement mixture. Cement, fly-ash, silica fume, and sand were first dry mixed for 3 min. Water was added and mixed for 3 min, and then super-plasticizer was added gradually and mixed for another 5 to 10 min. The amount of super-plasticizer for each matrix was predetermined to prevent fiber gravitation and to maintain uniform fiber distribution during mixing and casting, as provided in Table 1.

Cube type specimens measuring $50\times50\times50$ mm^3 were prepared to estimate the packing density of mortar matrices. The detailed procedure was described by Wong and Kwan [15]. In preparing single fiber pullout test specimens, a fiber was pre-installed in a holding device to control its embedded length and inclination angle; then the mortar was gradually poured into molds. For tensile and flexural specimens, fibers were dispersed by hand into the mortar mixture when the mortar started to show adequate flow and viscosity. Then, the mortar mixture with fibers was carefully placed in molds for tensile and flexural specimens using a wide scoop. No vibration was required, since the mixture with fibers was self-consolidating. All specimens were covered with plastic sheets and stored at room temperature for 24 h prior to demolding. After demolding, the specimens were placed in a water tank for an additional 2 weeks. All specimens were tested in a dry condition at the age of 17 days, which allowed 3 days for drying in the laboratory environment.

2.2. Test setup and parameters describing the test results

The pullout test setup and parameters characterizing the interfacial bond strength of H- and T-fibers are illustrated in Fig. 3. The section of

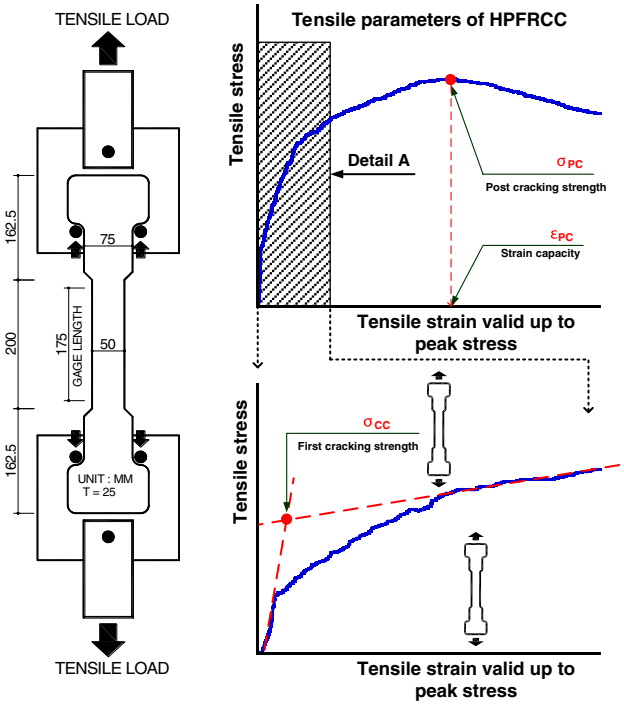

Fig. 4. Tensile test setup and parameters.

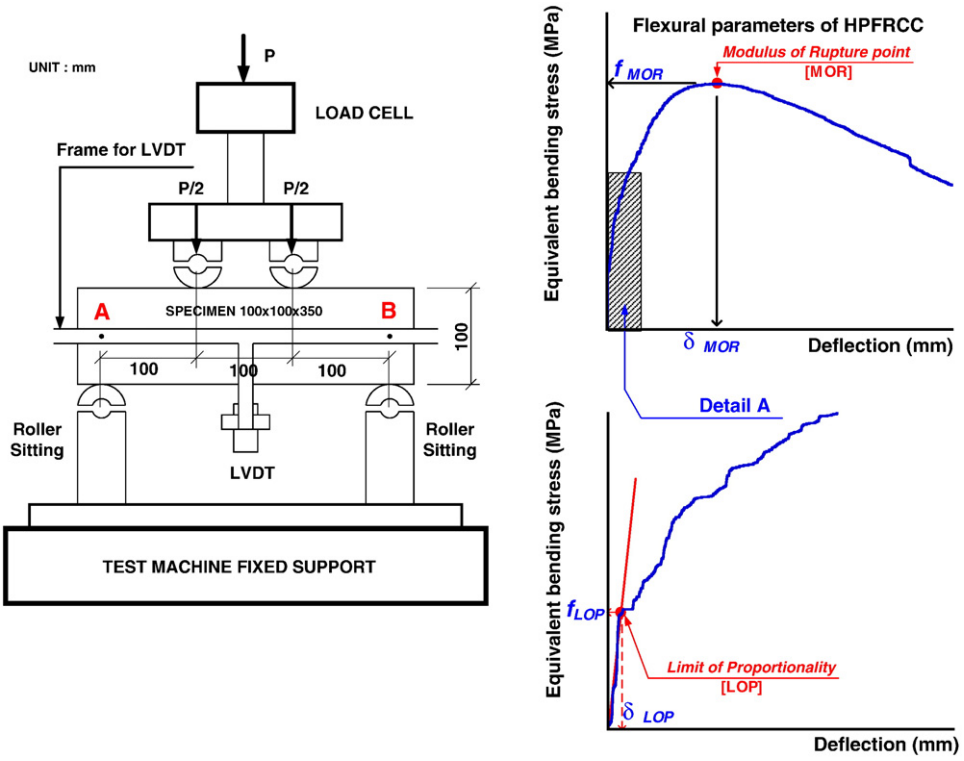

Fig. 5. Bending specimen geometry and test setup.

pullout specimen was 25×25 mm^2 and the fiber was embedded in the center of the specimen. The embedment length of fiber investigated was 15 mm, which was half the fiber length.

The maximum pullout load is identified as P_{max}, as shown in Fig. 3. The bond strength at maximum pullout load was calculated using Eq. (1).

$$\tau_{max} = \frac{P_{max}}{\pi \cdot d_f \cdot L_{em.}} \tag{1}$$

where τ_{max} is the bond strength at maximum pullout load, P_{max} is the maximum pullout load, d_f is the equivalent diameter of fiber, and $L_{em.}$ is the embedded length of fiber.

The pullout work during fiber pullout, as illustrated in Fig. 3, was also used to estimate equivalent bond strength using Eq. (2) [12].

$$\tau_{equiv.} = \frac{2 \cdot PW}{d_f \cdot L_{em.}^2} \tag{2}$$

where $\tau_{equiv.}$ is equivalent bond strength, PW is the pullout work until the complete pullout of fiber, d_f is the diameter of fiber, and $L_{em.}$ is the embedded length of fiber.

The tensile test setup and parameters for the tensile behavior of HPFRCC are shown in Fig. 4. A bell shaped tensile specimen was used. The cross section of the specimen was 50×25 mm^2 and the gage length

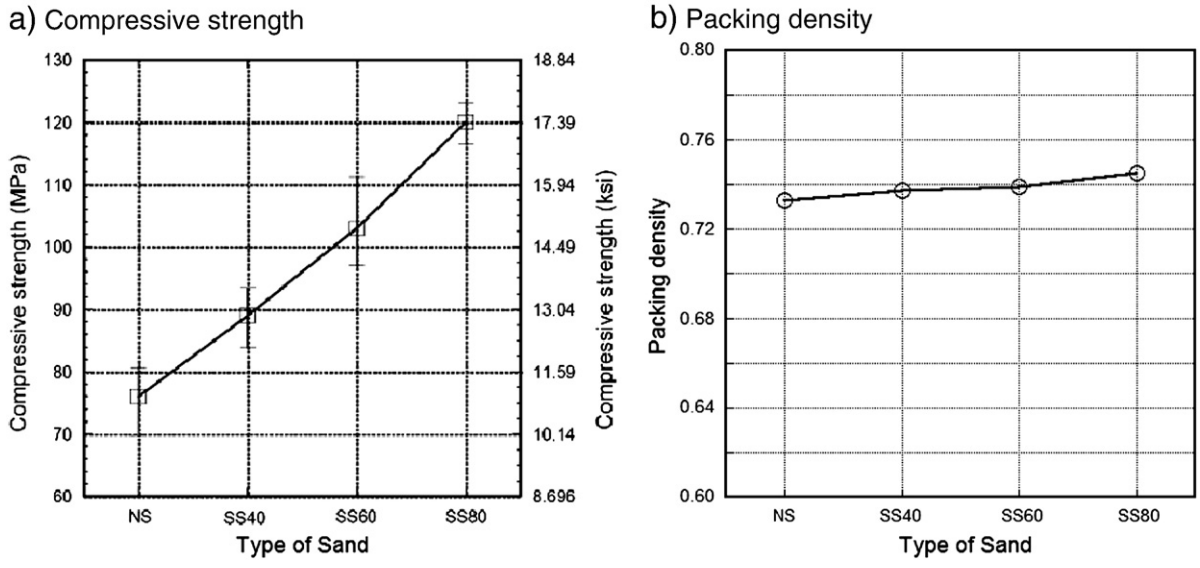

Fig. 6. Influence of sand grain size on: (a) compressive strength and (b) packing density.

used in the measurement of elongation was 175 mm. The parameters include first cracking strength, σ_{cc}, post cracking strength, σ_{pc}, and strain capacity, ε_{pc}. In addition to those parameters, the number of cracks within the gage length, averaged crack spacing, and consequent averaged crack width was investigated.

The flexural test specimen and setup were prepared according to ASTM standard C1609/C 1609M – 05 [8], as shown in Fig. 5. Details of the testing procedures can be found in ASTM standard C1609. A linear variable differential transformer was installed in an aluminum cage and used to measure the center deflection, as illustrated in Fig. 5. Parameters for the flexural behavior of HPFRCC are also shown in Fig. 5: the point where the nonlinear response begins is identified as the limit of proportionality (LOP), while the point with maximum flexural load is identified as modulus of rupture (MOR). The equivalent bending stress was estimated using Eq. (3), according to the ASTM standard. The area under the load–deflection curve was also estimated as flexural toughness (FT): e.g., the area under the curve until the deflection reaches δ_{MOR} is identified as FT_{MOR}.

$$f = \frac{P \cdot L}{b \cdot h^2} \tag{3}$$

where f is equivalent bending strength, P is the applied load, L is the span length of specimen, b is the width of the specimen, and h is the height of the specimen.

The packing density, denoted by ϕ in Eq. (4), is defined as the volume ratio of the solid components (V_c) in Eq. (5) and the whole volume of mortar matrix (V). The equations to estimate the wet packing density of the mortar matrix were proposed by Wong and Kwan [15].

$$\phi = V_c / V \tag{4}$$

$$V_c = \frac{M}{\rho_W u_W + \rho_C R_C + \rho_S R_S + \rho_{SF} R_{SF} + \rho_{FA} R_{FA}} \tag{5}$$

where M is the mass of the whole mortar matrix within a cube mold; ρ_w is the density of water; ρ_C, ρ_S, ρ_{SF}, and ρ_{FA} are the solid densities of cement, sand, silica fume, and fly ash, respectively; u_w is the volume ratio of the water to the granular material; and R_C, R_S, R_{SF} and R_{FA} are the volumetric ratios of cement, sand, silica fume and fly ash, respectively, to the total cementitious materials.

Table 3
Average values of pullout parameters.

Fiber type	Sand type	Maximum pullout stress (MPa)	Maximum bond stress (MPa)	Pullout work (N-mm)	Equivalent bond stress (MPa)
Hooked	NS	1574.788	9.842	665.867	5.024
	SS40	1636.877	10.231	701.693	5.294
	SS60	1708.291	10.677	757.578	5.716
	SS80	1859.269	11.930	802.288	6.053
Twisted	NS	1252.726	6.264	767.754	7.241
	SS40	1505.656	7.528	882.787	8.326
	SS60	1827.570	9.138	1189.471	11.218
	SS80	2151.539	10.758	1253.956	11.827

3. Results and discussion

3.1. Packing density and compressive strength

The influence of sand grain size on the packing density and compressive strength of mortar matrices is illustrated in Fig. 6 and summarized in Table 1. The size of sand grain only slightly affected the packing density; however, the consequent effect on compressive strength was significant, as demonstrated in Fig. 6. As the size of sand grain decreased from NS to SS80 in the composition of the mortar matrix, the packing density of the mortar matrix increased from 0.733 to 0.745 (2% increase) while the compressive strength increased from 76 MPa to 120 MPa (58% increase). Thus, the improved compressive strength of mortar with a finer sand grain cannot be fully explained by the packing density alone. The sand grain, or aggregate, generally provides a surface for nucleation of crystalline solid material [10]; thus, the reactivity of silicious aggregate increases as the sand grain becomes finer. Cordon and Gillespie [20] also reported that the compressive strength of concrete with a low water–cement ratio could be increased considerably by decreasing the size of aggregate. The significant enhancement in compressive strength associated with finer sand particles can be explained partly by the enhanced packing density and mainly by the more intensive pozzolanic reaction that increases the density of the CSH. Jo et al. [9] investigated the microstructure of mortar containing nano-SiO_2 and observed that this mortar produced a much denser

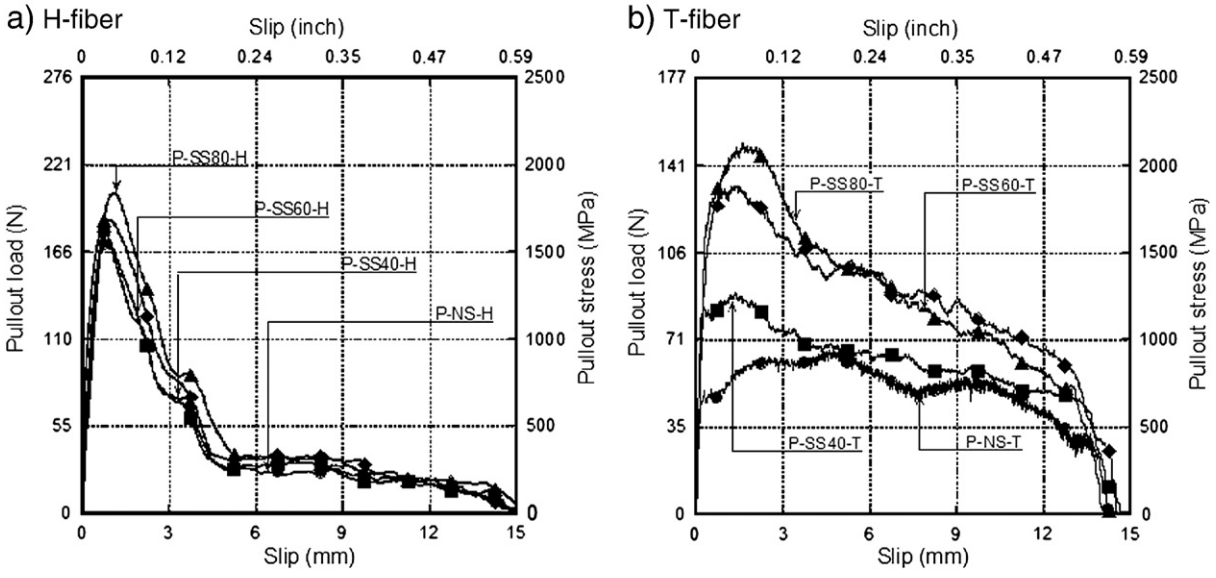

Fig. 7. Pullout stress versus slip curves according to the type of sand.

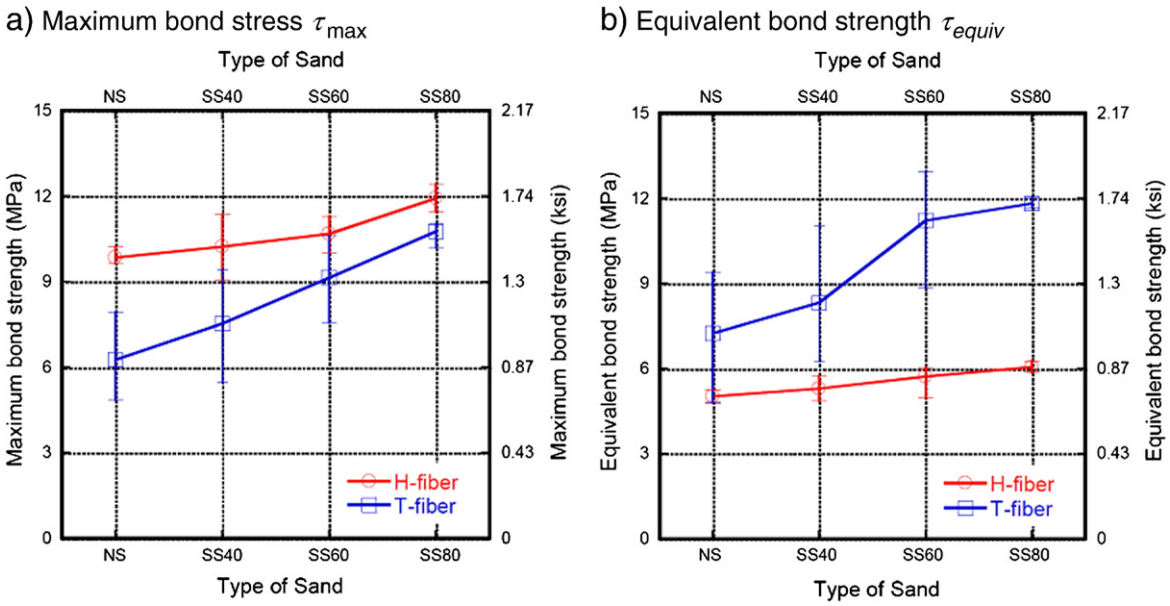

Fig. 8. Influence of sand grain size on bond strength.

formation of hydration products. The microstructure of mortar mixture according to the size of sand grain will be further studied in a future project.

3.2. Interfacial bond properties from single fiber pullout

The averaged pullout load (or stress) versus slip curves according to the size of sand grain is provided in Fig. 7a and b, for H- and T-fibers, respectively. The curve for each series was averaged from at least three pullout test results. It is clear from Fig. 7 that the pullout resistance of both fibers was noticeably improved by a decrease in the size of sand grain. In addition, the improvement in both pullout stress and pullout energy differed according to the type of fiber. Hence, the effect of the size of sand grain depends on the type of fiber, i.e. the different pullout mechanisms of fibers. H- and T-fibers have totally different pullout mechanisms: H-fibers use the plastic energy generated from two plastic hinges at the hooked end during fiber pullout, while T-fibers utilize the untwisting torsion moment resistance of the fiber. Thus, H-fiber uses

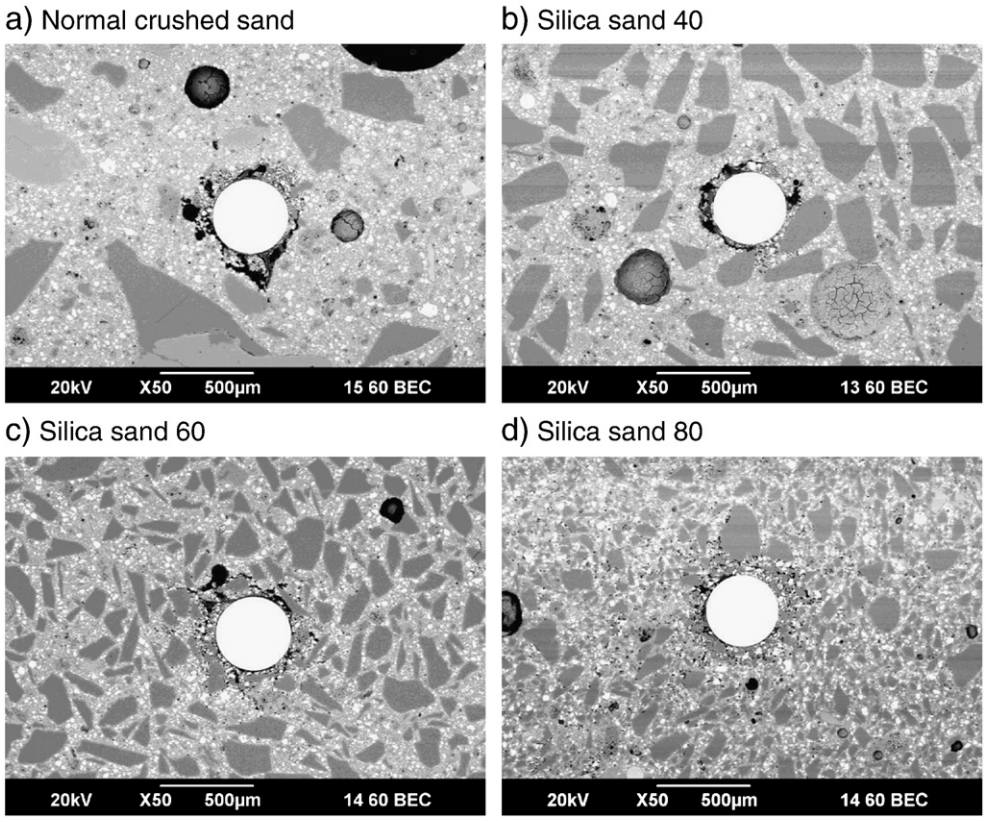

Fig. 9. Backscattered electron (BSE) images according to different types of sand.

only a relatively small portion of the fiber's embedded length, whereas T-fiber uses the entire embedded length of the fiber for generating mechanical bond strength [4,5,13,16].

The averaged numerical values of fiber pullout parameters for the interfacial bond properties are summarized in Table 3. The parameters include maximum fiber pullout stress, $\sigma_{f,\max}$, maximum bond strength, $\tau_{\max}$, pullout work, *PW*, and equivalent bond strength, $\tau_{equiv.}$. The numerical values are also averaged from at least three specimens. The definitions are provided in Fig. 3.

As the size of sand grain decreased from NS to SS80, the $\sigma_{f,\max}$ of H-fiber increased from 1575 MPa to 1859 MPa (18% increase) while that of T-fiber showed a much greater enhancement, from 1253 MPa to 2152 MPa (72% increase). In particular, the $\sigma_{f,\max}$ (2152 MPa) of T-fiber in the SS80 matrix was close to the ultimate tensile strength of the T-fiber investigated, while the $\sigma_{f,\max}$ of T-fiber in the NS matrix was only 1253 MPa. The *PW* of H-fiber increased from 665.87 N-mm to 802.29 N-mm (20% increase) as the size of sand grain decreased, while the *PW* of T-fiber showed a 63% increase, from 767.75 N-mm to 1253.96 N-mm.

The influence of sand fineness on bond strength $\tau_{\max}$ and $\tau_{equiv.}$ is shown in Fig. 8a and b, respectively. The improvement in both $\tau_{\max}$ and $\tau_{equiv.}$ as the sand grain became finer from NS to SS80 was much higher for T-fiber than for H-fiber. In addition, the $\tau_{equiv.}$ of T-fiber was higher than that of H-fiber, while the $\tau_{\max}$ of T-fiber was lower than that of H-fiber. The $\tau_{equiv.}$ of T-fiber increased from 7.241 MPa to 11.827 MPa (63% increase) as the sand grain became

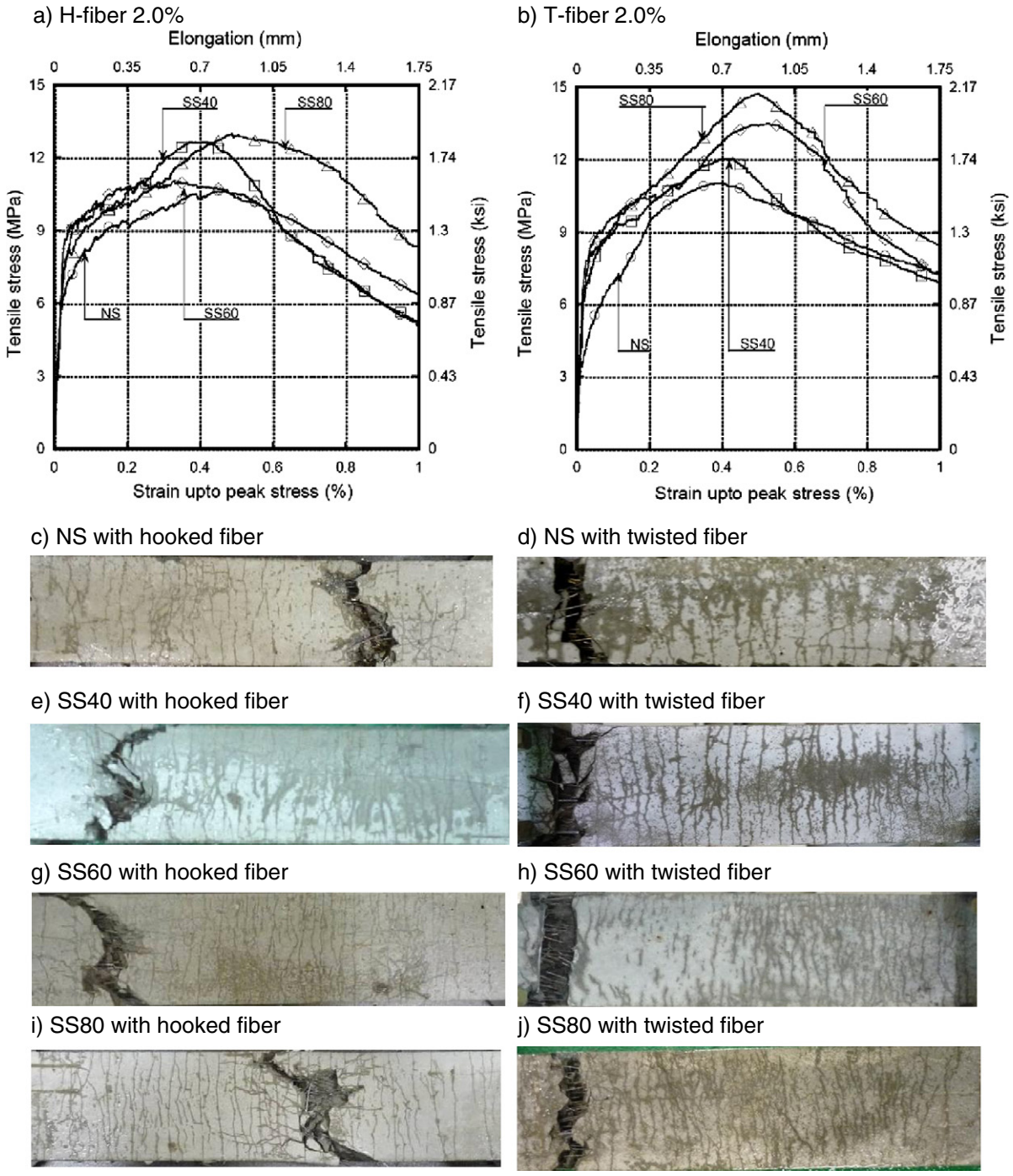

Fig. 10. Tensile stress versus strain curves according to the type of sand.

Table 4
Average values of tensile parameters.

Fiber type	Sand type	First cracking		Post cracking		Number of cracks within 175 mm gage length (EA)	Average crack spacing (mm)	Average crack width (μm)
		Strain (%)	Stress (MPa)	Strain (%)	Stress (MPa)			
Hooked	NS	0.020	7.814	0.451	10.738	18	9.913	44.7
	SS40	0.025	8.744	0.403	12.906	32	5.472	22.0
	SS60	0.041	9.445	0.422	11.382	34	5.240	21.9
	SS80	0.051	8.653	0.546	13.255	42	4.173	22.7
Twisted	NS	0.105	7.506	0.411	11.334	23	7.681	31.3
	SS40	0.037	7.550	0.414	12.096	25	6.924	28.6
	SS60	0.031	8.074	0.503	13.849	37	4.782	24.0
	SS80	0.035	8.447	0.532	14.906	43	4.120	21.9

finer from NS to SS80, while that of H-fiber increased only from 5.024 MPa to 6.053 MPa (20% increase).

Based on the analysis of the fiber pullout test results, it is clear that interfacial bond properties are very much influenced by the size of sand grain and can be significantly improved by using finer sand grains in the matrix surrounding the fibers. As the sand grains become finer, the vacant space surrounding the fibers decreases, while the packing density of the matrix surrounding the fibers increases. Thus, the volume

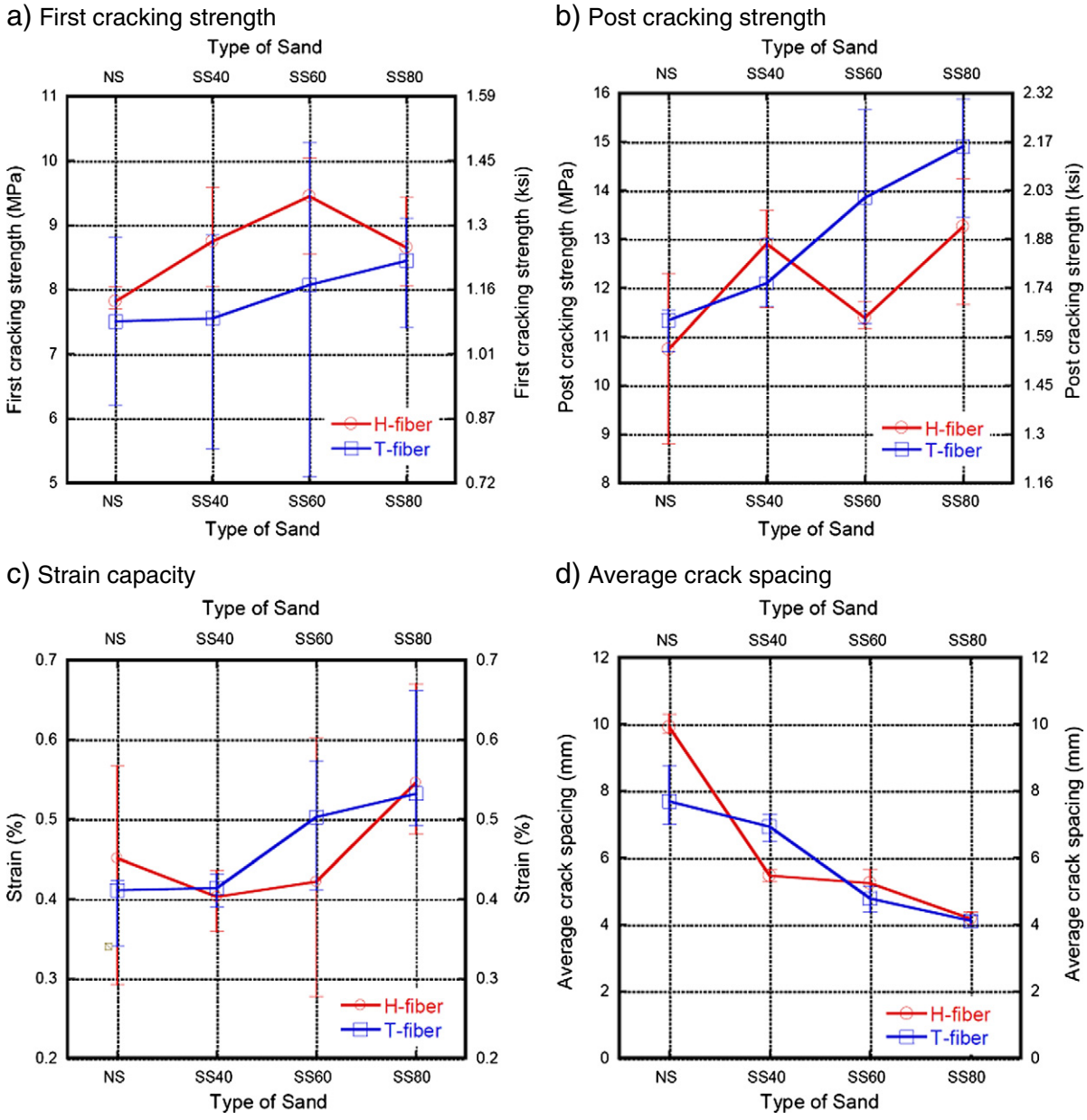

Fig. 11. Influence of sand grain size on tensile parameters of HPFRCC.

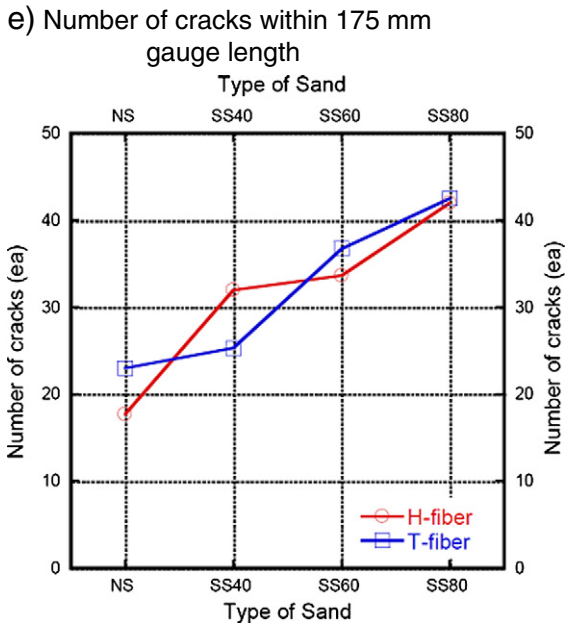

Fig. 11 (*continued*).

occupied by sand grains in the part of the matrix close around the fiber increases for finer grains. This increase in the proportion of sand grains at the interface between the fiber and matrix can be expected to increase the local stiffness of the matrix and to decrease porosity, as illustrated in the backscattered electron images shown in Fig. 9, which were recorded before fiber pullout. The higher stiffness and low porosity of the interface are thought to be the main reason for the enhanced pullout resistance (bond strength) of the fibers in a matrix with finer sand grains. This also explains why the pullout behavior of T-fiber shows a more sensitive response to sand fineness, because of its more intensive mechanical interaction at the interface between fiber and matrix.

3.3. Tensile behavior of HFPRCC

Fig. 10 shows tensile stress–strain curves and photographs illustrating the multiple micro cracking behavior for each tensile test series. The averaged curve per series was obtained from at least three specimens. As shown in Fig. 10, the use of finer sand in the matrix improves the overall tensile and multiple cracking behavior of HPFRCC with high-strength deformed steel fibers. The averaged numerical values of the tensile parameters are summarized in Table 4. These numerical values are also averaged from at least three specimens.

Tensile parameters, including first cracking strength, post cracking strength, and strain capacity of HPFRCC were defined in Fig. 4, and the influence of sand fineness on the tensile parameters is shown in Fig. 11. The improvement in first cracking strength was not as high as in post cracking strength, although there was a slight enhancement of first cracking strength as the size of sand grain decreased, as shown in Fig. 11a and b. The post cracking strength of HPFRCC with T-fibers when SS80 was used in the matrix was 31% higher than for NS, while that of HPFRCC with H-fibers was 23% higher. Thus, the post cracking strength showed a higher sensitivity to the size of sand grain in the T-fiber series than in the H-fiber series. T-fiber also showed a greater improvement in strain capacity than did H-fiber when SS80 was used instead of NS; 27% for T-fiber and 21% for H-fiber, as shown in Fig. 11c. Fig. 11d and e shows the influence of sand grain size on the number of micro cracks as well as averaged crack spacing.

In general, the series with T-fiber and SS80 showed the best tensile behavior, with better post cracking strength and strain capacity, and a greater number of micro cracks. The improved bond properties from using finer sand grain, due to the higher local stiffness and denser microstructure at the interface, were clearly translated into tensile behavior.

3.4. Flexural behavior of HFPRCC

Fig. 12 shows the equivalent bending stress versus deflection curves for each test series, while Fig. 13 shows the influence of sand fineness on flexural parameters. The averaged curve was obtained from at least three specimens. The averaged numerical values of several parameters related to the flexural response of HPFRCC, e.g., equivalent bending

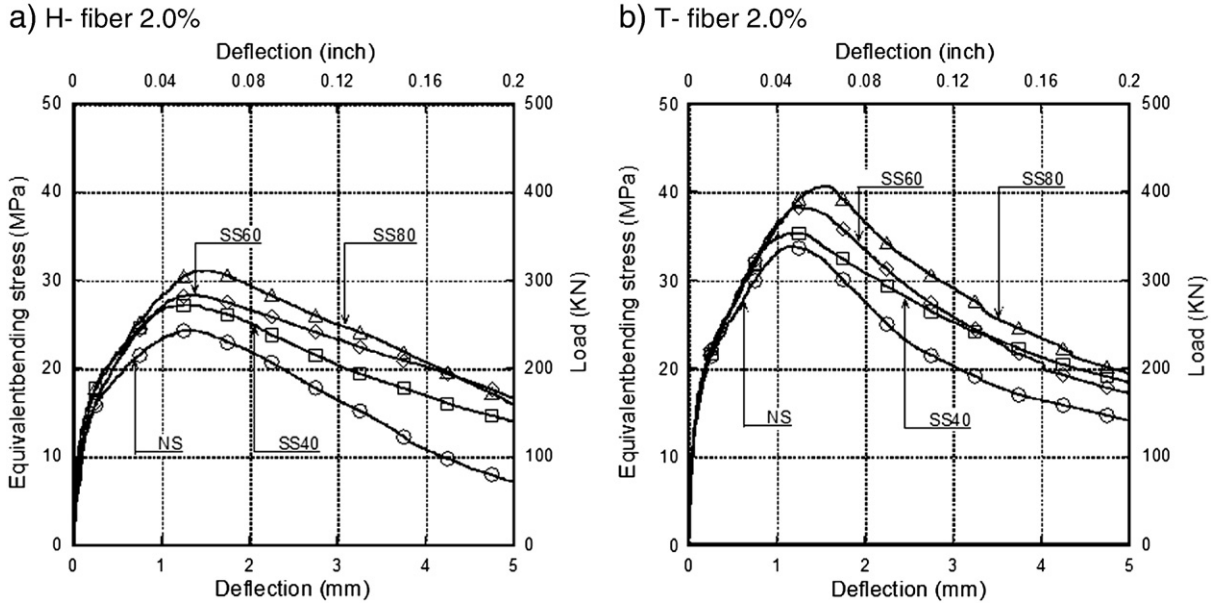

Fig. 12. Equivalent bending stress versus deflection curves according to the type of sand.

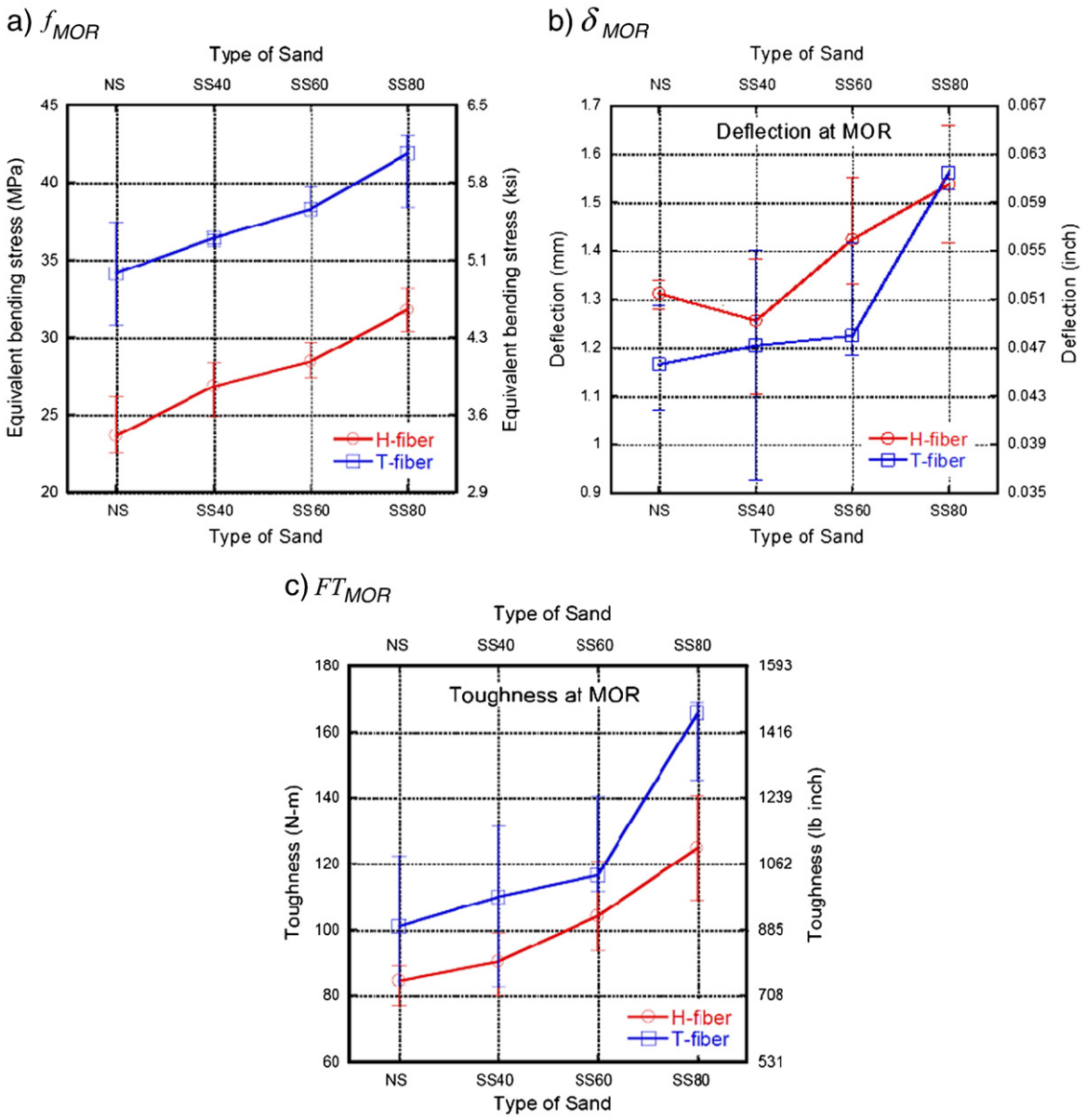

Fig. 13. Influence of sand grain size on flexural behavior of HPFRCC.

stress, deflection and toughness at LOP and MOR, are summarized in Table 5. These numerical values are also averaged from at least three specimens.

The bending strength at LOP (f_{LOP}) was between 8.343 MPa and 10.467 MPa for H-fiber, and 12.411 MPa and 12.784 MPa for T-fiber. f_{LOP} showed little sensitivity to sand fineness, while f_{MOR} was more sensitive in all series, as shown in Fig. 13a. As the size of sand grain became finer from NS to SS80, the f_{MOR} of series with H-fiber increased from 24.64 MPa to 31.78 MPa (29% increase), while the f_{MOR} of series with T-fiber showed only a 19% increase, from 34.14 MPa to 40.71 MPa. Deflection at MOR (δ_{MOR}) was also sensitive to the size of sand grain, as shown in Fig. 13b. The δ_{MOR} for H-fiber increased from 1.312 mm to 1.539 mm (17% increase) as the sand particle size decreased from NS to SS80, whereas the δ_{MOR} for the series with T-fiber showed a greater improvement, from 1.166 mm to 1.550 mm (32% increase). Toughness at MOR (FT_{MOR}) was also extremely sensitive to the size of sand grain, as shown in Fig. 13c. The series with H-fiber showed a 47% increase in FT_{MOR}, from 84.609 N-m to 124.728 N-m, while the series with T-fiber demonstrated a 57% increase, from 101.139 N-m to 158.867 N-m. In comparison with H-fiber, the flexural behavior of T-fiber HPFRCC thus showed greater sensitivity to the size of sand grain.

In general, the test series with T-fibers produced better flexural performance and higher sensitivity to the size of sand grain than those with H-fibers.

4. Conclusions

This study investigated the effect of sand grain size on the mechanical properties and multiple crack formation of HPFRCC with high-strength deformed steel fibers, such as hooked (H-) and twisted (T-) fibers. Four types of sand with different sand grain sizes were investigated: normal crushed sand (NS), micro silica sand (SS40), fine micro silica sand (SS60), and very fine micro silica sand (SS80). Although both H- and T-fibers showed sensitive behavior according to the size of sand grain, T-fiber showed a higher sensitivity than H-fiber as regards fiber pullout, and the tensile and flexural behavior of HPFRCC with those fibers. The difference could be attributed to the greater mechanical interaction between fiber and matrix based on the T-fiber's unique

Table 5
Average values of flexural parameters.

Fiber type	Sand type	Limit of proportionality [LOP]			Modulus of rupture [MOR]		
		δ (mm)	f (MPa)	Toughness (N-m)	δ (mm)	f (MPa)	Toughness (N-m)
Hooked	NS	0.048	8.343	0.757	1.312	24.637	84.609
	SS40	0.038	8.420	0.655	1.257	26.840	90.344
	SS60	0.065	7.586	0.937	1.424	28.428	104.176
	SS80	0.041	10.467	0.956	1.539	31.776	124.728
Twisted	NS	0.066	12.784	1.655	1.166	34.142	101.139
	SS40	0.063	12.761	1.671	1.205	36.402	110.010
	SS60	0.050	12.411	1.276	1.289	38.750	124.461
	SS80	0.052	12.546	1.404	1.550	40.711	158.867

untwisting pullout mechanism. The following observations and conclusions can be drawn from the experimental study:

1. As the size of sand grain in a mortar matrix decreased, its packing density increased slightly, from 0.733 to 0.745 (2%). However, the compressive strength of a mortar matrix with this slightly increased packing density was significantly enhanced, from 76 MPa to 120 MPa (58%). The improvement in compressive strength from using finer sand grain is mainly the result of the increased density of CSH due to the larger surface area of silicious aggregate, and cannot be explained by the higher packing density alone.
2. The use of finer grain sand produces favorable effects on both the tensile and flexural behavior of HPFRCC with high-strength deformed steel fibers, since the finer sand grain enhances the interfacial bond strength as a result of the higher local stiffness and low porosity at the interfacial transition zone.
3. High strength steel twisted (T-) fibers showed a higher sensitivity to the size of sand grain than did high-strength steel hooked (H-) fibers, although both T- and H-fibers demonstrated enhanced performance in fiber pullout, tensile and flexural tests as the size of sand grain decreased. The observed difference in sensitivity can be attributed to the different fiber pullout mechanisms.
4. The use of normal crushed sand (NS) in HPFRCC with high-strength deformed steel fibers also successfully produces tensile strain hardening behavior accompanied by multiple micro cracks. The tensile performance of HPFRCC with NS is quite comparable to that of HPFRCC with silica sands: 76–81% for post cracking strength, 77–83% for strain capacity, and 43–53% for multiple cracks.

There is a clear correlation between the local stiffness and porosity of ITZ resulting from the different size of sand grain and fiber pullout behavior (interfacial bond strength). That correlation will be the subject of a future publication by the authors.

Acknowledgments

This research was the product of a research collaboration between the Advanced Cement Composite Lab. in Sejong University, South Korea, and the Innovative Construction Materials Eng., IIS, at The University of Tokyo, Japan. This research was sponsored by the Human Resources Development (20104010100520) and research project (2010161010004K) granted by the Korea Institute of Energy Technology Evaluation and Planning. The opinions expressed in this paper are those of the authors and do not necessarily reflect the views of the sponsors.

References

[1] A. Bentur, M.G. Alexander, A review of the work of the RILEM TC159-ETC: engineering of the interfacial transition zone in cementitious composites, Mater. Struct. 33 (2) (2000) 82–87.
[2] A. Elsharief, M.D. Cohen, J. Olek, Influence of aggregate size, water cement ratio, and age on the microstructure of the interfacial transition zone, Cem. Concr. Res. 33 (2003) 1837–1849.
[3] A.E. Naaman, H.W. Reinhardt, Proposed classification of FRC composites based on their tensile response, Mater. Struct. 39 (5) (June 2006) 547–555.
[4] A.E. Naaman, Engineered steel fibers with optimal properties for reinforcement of cement composites, J. Adv. Concr. Technol. 1 (3) (November 2003) 241–252 Japan Concrete Institute.
[5] A.E. Naaman, Fibers with slip hardening bond, high performance fiber reinforced cement composites 3, in: H.W. Reinhardt, A.E. Naaman (Eds.), RILEM Proceedings, Pro. 6, Cachan, France, May 1999, pp. 371–385.
[6] A.E. Naaman, Private e-mail discussion, 2010.
[7] A.E. Naaman, Toughness, ductility, surface energy and deflection—hardening FRC composites, Proceedings of JCI Workshop on Ductile Fiber Reinforced Cementitious Composites (DFRCC)—Application and Evaluation, Japan Concrete Institute, Tokyo, Japan, Oct. 2002, pp. 33–57.
[8] ASTM C 1609/C 1690 M – 05, Standard Test Method for Flexural Performance of Fiber Reinforced Concrete (Using Beam with Third-point Loading), American Society of Testing and Materials, Jan. 2006, pp. 1–8.
[9] B.W. Jo, C.H. Kim, G.H. Tae, J.B. Park, Characteristics of cement mortar with nano-SiO_2 particles, Constr. Build. Mater. 21 (6) (2007) 1351–1355.
[10] D. Zampini, S.P. Shah, H.M. Jennings, Early age microstructure of the paste–aggregate interface and its evolution, J. Mater. Res. 13 (7) (1998) 1888–1898.
[11] D.J. Kim, S.H. Kang, Influence of sand fineness on tensile behavior of high performance fiber reinforced cement composites for containment building, Proceedings of the International Congress on Advance in Nuclear Power Plants 2011, Nice, France, May 2–5 2011, pp. 2301–2308.
[12] D.J. Kim, S. El-Tawil, A.E. Naaman, Correlation between single fiber pullout behavior and tensile response of FRC composites with high strength steel fiber, Proceedings of the Fifth International Workshop of High Performance Fiber Reinforced Cementitious Composites, RILEM Proceedings, Pro. 53, S.A.R.L., Cachan, France, July 2007, pp. 67–76.
[13] D.J. Kim, S. El-Tawil, A.E. Naaman, Loading rate effect on pullout behavior of deformed steel fibers, ACI Mater. J. 105 (65) (November 2008) 576–584.
[14] D.J. Kim, S.H. Kang, T.-H. Ahn, Influence of sand fineness on self healing behavior of high performance fiber reinforced cementitious composites, Proceedings of the Japan Concrete Institute Annual Conference, Osaka, Japan, July 12–14 2011, pp. 275–280.
[15] H.H.C. Wong, A.K.H. Kwan, Packing density of cementitious materials: part 1—measurement using a wet packing model, Mater. Struct. 41 (4) (2008) 689–701.
[16] J.M. Alwan, A.E. Naaman, P. Gurrero, Effect of mechanical clamping on the pullout response of hooked steel fibers embedded in cementitious matrices, Concr. Sci. Eng. 1 (March 1999) 15–25.
[17] M. Sahmaran, M. Lachemi, K.M.A. Hossain, V.C. Li, Influence of aggregate type and size on ductility and mechanical properties of engineered cementitious composites, ACI Mater. J. 106 (3) (2009) 308–316.
[18] P. Gurrero, A.E. Naaman, Effect of mortar fineness and adhesive agents on pullout response of steel fibers, ACI Mater. J. 97 (1) (2000) 12–22.
[19] S. Igarashi, A. Bentur, S. Mindess, The effect of processing on the bond and interfaces in steel reinforced cement composites, Cem. Concr. Compos. 18 (5) (1996) 312–322.
[20] W.A. Cordon, H.A. Gillespie, Variables in concrete aggregate and Portland cement paste which influence the strength of concrete, J. Am. Concr. Inst. Proc. 60 (8) (1963) 1029–1050.
[21] A.E. Naaman, H.W. Reinhardt, Characterization of high performance fiber reinforced cement composites, in: A.E. Naaman, H.W. Reinhardt (Eds.), High performance fiber reinforced cement composites: HPFRCC 2. Proceedings of 2nd international workshop on HPFRCC, Chapter 41, RILEM, No. 31, E. & FN Spon, London, 1996, pp. 1–24.